VIP Nanocomposites Very Important Paper

Deutsche Ausgabe: DOI: 10.1002/ange.201603189
Internationale Ausgabe: DOI: 10.1002/anie.201603189

Chemical-Bonding-Directed Hierarchical Assembly of Nanoribbon-Shaped Nanocomposites of Gold Nanorods and Poly(3-hexylthiophene)

Shuang Pan, Luze He, Juan Peng, Feng Qiu, and Zhiqun Lin**

Abstract: *Nanoribbon-shaped nanocomposites composed of conjugated polymer poly(3-hexylthiophene) (P3HT) nanoribbons and plasmonic gold nanorods (AuNRs) were crafted by a co-assembly of thiol-terminated P3HT (P3HT-SH) nanofibers with dodecanethiol-coated AuNRs (AuNRs-DDT). First, P3HT-SH nanofibers were formed due to interchain π–π stacking. Upon the addition of AuNRs-DDT, P3HT-SH nanofibers were transformed into nanoribbons decorated with the aligned AuNRs on the surface (i.e., nanoribbon-like P3HT/AuNRs nanocomposites). Depending on the surface coverage of the P3HT nanoribbons by AuNRs, these hierarchically assembled nanocomposites exhibited broadened and red-shifted absorption bands of AuNRs in nIR region due to the plasmon coupling of adjacent aligned AuNRs and displayed quenched photoluminescence of P3HT. Such conjugated polymer/plasmonic nanorod nanocomposites may find applications in fields, such as building blocks for complex superstructures, optical biosensors, and optoelectronic devices.*

The ability to tailor hierarchical bottom-up assembly of organic and inorganic nanomaterials and yield complex architectures offers exceptional potential in developing complex and functional nanocomposites for use in optics, electronics, optoelectronics, sensors, catalysis, magnetic materials and devices.[1] In this context, nanoribbon-shaped organic/inorganic nanocomposites have garnered increasing attention in recent years.[2] Organic/inorganic nanocomposites comprising polymers and nanocrystals combine advantages of light-weight, flexibility, processibility and low-cost of polymers, and strongly size-dependent physical properties peculiar to nanocrystals. They often exhibit intriguing new structures, properties, and functionalities.[3] Moreover, self-assembly of these nanocomposites into nanoribbon-shaped structures with high aspect ratios can further lead to materials with collective properties dictated by their dimensions. This has been the subject of much research.

Poly(3-hexylthiophene) (P3HT) is one of most widely studied conjugated polymers owing to its high charge-carrier mobility and solution structural diversity. P3HT can self-assemble to form a set of interesting structures such as fibers, ribbons, and sheets.[4] Recently, P3HT has been either placed in direct contact with quantum dots and rods by chemical coupling to produce P3HT/semiconductor nanocomposites[5] or hybridized with nanoparticles in a controllable manner.[6] As an important anisotropic building block, gold nanorods (AuNRs) continue to receive considerable interest for the preparation of nanoscale photonic, electronic, sensory, and biological imaging devices because of their unique size- and shape-dependent optical properties.[7] Co-assembly of P3HT and AuNRs into nanoribbon-shaped nanocomposites is not only of fundamental importance in improving our understanding of self-assembly processes but also of practical interest for building functional nanocomposite materials. It is worth noting that despite a few elegant studies on nanoribbon-like conjugated polymer/nanoparticle nanocomposites,[8] hierarchically assembled nanoribbon-shaped nanocomposites composed of P3HT and AuNRs have not yet been explored.

Herein, we report a robust, hierarchical bottom-up assembly strategy for creating nanoribbon-shaped P3HT/AuNRs nanocomposites. First, thiol-terminated P3HT (P3HT-SH) chains self-assemble into P3HT-SH nanofibers with edge-on orientation via interchain π–π stacking. Subsequently, the addition of AuNRs to P3HT-SH nanofiber solution triggers the formation of P3HT/AuNRs nanoribbons driven by the presence of a small amount of dodecanethiol (DDT) (i.e., free DDT dissociated from DDT-coated AuNRs (AuNRs-DDT) surface). Interestingly, AuNRs are aligned concurrently along the long axis of P3HT-SH nanoribbons via the Au–S bonding to yield nanoribbon-shaped P3HT/AuNRs nanocomposites (i.e., a hierarchical assembly comprising aligned AuNRs in close proximity within P3HT-SH nanoribbons that are submicron wide and a few to tens of micron long and comprising stacked, vertically oriented P3HT-SH chains). Quite intriguingly, when P3HT-SH nanoribbons and nanofibers coexist, AuNRs and Au nanoparticles (AuNPs) are found to selectively decorate the P3HT-SH nanoribbons and nanofibers, respectively. Clearly, the use of Au nanocrystals of different shapes stands out an effective means of identifying the architectures of P3HT-SH (i.e., nanoribbons vs. nanofibers). It is notable that these nanoribbon-shaped P3HT/AuNRs nanocomposites exhibit the broadened and red-shifted absorptions of AuNRs in near infrared region due

[*] S. Pan, L. He, Prof. J. Peng, Prof. F. Qiu
State Key Laboratory of Molecular Engineering of Polymers, Collaborative Innovation Center of Polymers and Polymer Composite Materials, Department of Macromolecular Science, Fudan University
Shanghai 200433 (China)
E-mail: juanpeng@fudan.edu.cn
Prof. Z. Lin
School of Materials Science and Engineering, Georgia Institute of Technology
Atlanta, GA 30332 (USA)
E-mail: zhiqun.lin@mse.gatech.edu

Supporting information for this article can be found under: http://dx.doi.org/10.1002/anie.201603189.

to the plasmon coupling of adjacent aligned AuNRs and quenched photoluminescence of P3HT, depending sensitively on the coverage of AuNRs on the P3HT-SH nanoribbon surface. This simple strategy may be potentially applicable to assemble other conjugated polymers and inorganic nanorods into new functional composite materials with unique optical, electronic, optoelectronic and even collective properties.

P3HT-SH ($M_n = 7200$, $M_w/M_n = 1.08$) was first synthesized by Grignard metathesis polymerization (GRIM) of activated monomer 2-bromo-5-iodo-3-hexylthiophene (M1).[9] Subsequently, the reaction mixture was divided into two portions with one quenched using sulfur powder and the other quenched with 5 M HCl. Notably, their matrix-assisted laser desorption/ionization-time of flight (MALDI-TOF) mass spectra showed a mass difference of 32, confirming the success in obtaining one-end SH-terminated P3HT chains by sulfur powder (see Experimental Section in Supporting Information and Figures S1–S4). P3HT-SH nanofibers were then prepared in the mixed solvents of $CH_2Cl_2/CHCl_3$ (7/1 by volume),[6] and had an average width of 13 nm and length of a few microns (Figure 1 a). The selected area electron diffraction (SAED; Figure 1 a) pattern showed a diffraction ring, which can be assigned to crystallographic (020) plane of P3HT with a d_{020}-spacing of 3.8 Å, confirming the π–π stacking of P3HT chains along (010) direction with the edge-on orientation of backbones (i.e., (001) direction) that are parallel to the substrate. It has been reported that below the critical molecular weight of 10 kDa, P3HT backbones adopt a fully extended chain conformation with the chain-ends located at the fibril edges.[10] In our study, the M_n of P3HT-SH is 7200 and the resulting P3HT-SH nanofibers have a width of 13 nm, which is consistent with the length of an extended P3HT chain. As a result, -SH groups are situated at the edge of each nanofiber (upper right part of Figure 1 g). This can be further confirmed by experiments described below. The AuNRs with a length of 64.4 ± 5.6 nm and width of 14.6 ± 2.6 nm coated with a double layer of cetyl trimethylammonium bromide (CTAB) were synthesized (i.e. AuNRs-CTAB; Figure 1 b)) using the seed-mediated growth method.[11] To disperse AuNRs in organic solvent, a ligand-exchange procedure using DDT as the ligand was performed to transfer AuNRs from aqueous solution to the $CH_2Cl_2/CHCl_3$ mixed solvents, yielding DDT-coated AuNRs (i.e., AuNRs-DDT).[12] Interestingly, in comparison with the well-dispersed AuNRs-CTAB, AuNRs-DDT were found to preferentially form side-by-side assemblies (Figure 1 c) due to the strong rod–rod attractive interaction driven by dipole–dipole and van der Waals interactions.[13]

Both P3HT-SH nanofiber and AuNRs-DDT $CH_2Cl_2/CHCl_3$ solutions were then thoroughly mixed under stirring for 24 h. Surprisingly, nanoribbon-shaped P3HT/AuNRs composed of aligned AuNRs over a large area were produced (Figure 1 d). The SAED pattern shown as inset displayed four diffraction rings which can be assigned to crystallographic (h00) ($h = 1,2,3$) and (020) planes of P3HT-SH, with a d_{100}-spacing of 16.7 Å and d_{020}-spacing of 3.8 Å, suggesting that P3HT-SH chains possess a flat-on orientation in nanoribbons with the P3HT backbone perpendicular to the surface of nanoribbon.[14] Figure 1 e shows a high-resolution transmission electron microscopy (HRTEM) image of AuNRs within the nanoribbon where AuNRs maintained a string-like end-to-end orientation. No P3HT-SH chains were observed in the HRTEM image due to the low electron density of P3HT-SH compared to AuNRs (Figure 1 e). The thickness of nano-

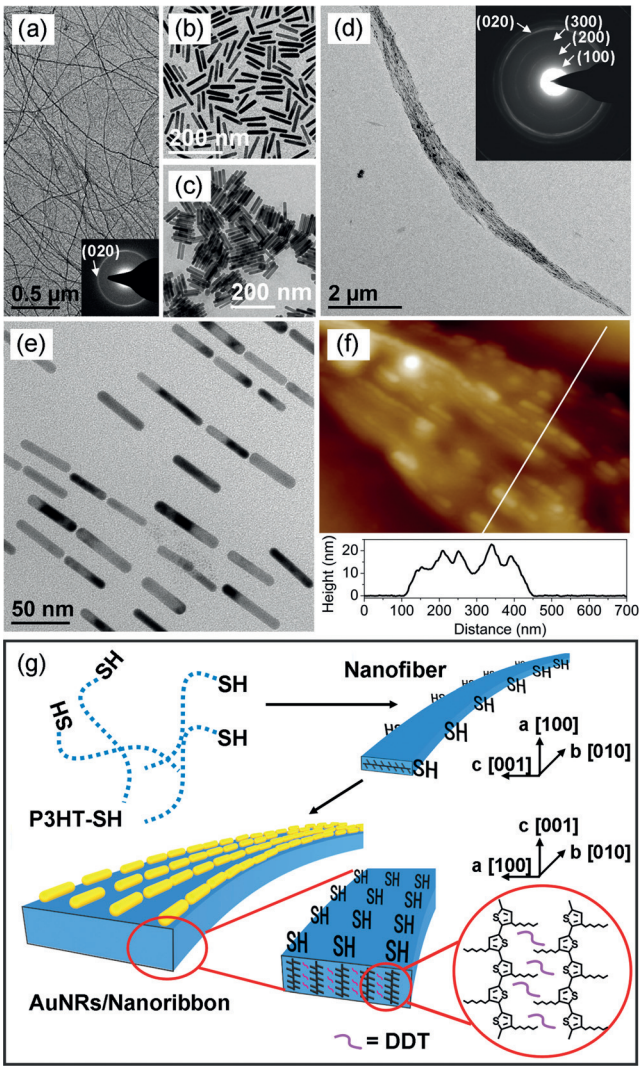

Figure 1. a)–e) Representative TEM images of a) SH-terminated P3HT (P3HT-SH) nanofibers yielded in $CH_2Cl_2/CHCl_3$ solution, b) AuNRs-CTAB synthesized in water, c) DDT-coated AuNRs (AuNRs-DDT) produced in $CH_2Cl_2/CHCl_3$ solution, d) P3HT/AuNRs nanoribbon-like nanocomposites formed by a co-assembly P3HT-SH and AuNRs-DDT, and e) close-up of (d) showing AuNRs aligned on the surface of P3HT-SH nanoribbon. The insets in (a) and (d) are the corresponding SAED patterns. f) AFM image (top panel) and the corresponding line profile (bottom panel) of P3HT/AuNRs nanoribbon-shaped nanocomposites. g) Stepwise representation of the formation of nanoribbon-shaped nanocomposites: P3HT-SH chains (top left) self-assemble into P3HT nanofibers via interchain π–π stacking with edge-on orientation (top right). The addition of AuNRs leads to the formation of P3HT/AuNRs nanoribbons (bottom) driven by the synergy of covalent interaction between AuNRs and terminal SH groups on P3HT-SH nanofibers and self-assembly of P3HT-SH nanofibers facilitated by the presence of minimal free DDT molecules dissociated from AuNRs-DDT (representing as red curves connecting two adjacent P3HT chains; right close-up).

ribbon is approximately 13 nm as measured by atomic force microscopy (AFM; Figure 1 f), which agreed well with the length of an extended P3HT chain, further substantiating that P3HT backbones are perpendicular to the substrate. Taken together, P3HT backbones transform from the parallel to perpendicular orientation during the morphological transition from nanofiber to nanoribbon. Accordingly, the location of terminal -SH groups on P3HT-SH changed from the edge in P3HT-SH nanofiber (upper right in Figure 1 g) to the surface of nanoribbon-shaped P3HT/AuNRs (lower right in Figure 1 g). These exposed -SH groups on the surface provide access to readily interact with AuNRs via the formation of Au–S bonds. This correlates well with the observation of aligned AuNRs on the surface of nanoribbons by TEM and AFM (Figure 1 e,f) due to the favorable Au–Au and Au–S interactions. Such nanofiber-to-nanoribbon transformation may be largely driven by the presence of a small amount of dissociated DDT ligands from the AuNRs surface (i.e., minimal free DDT). To verify this hypothesis, a certain amount of DDT was deliberately added in the P3HT-SH nanofiber solution, which induced the nanofiber-to-nanoribbon transformation (Figure S5). It has been reported that the thiol molecules adsorbed on the surface of inorganic nanoparticles are in a dynamic equilibrium with those present in solution.[15] Thus, even with repeated centrifugation and purification, minimal free DDT may still exist in the AuNR solution. We now turn our attention to further rationalize nanofiber-to-nanoribbon transformation as follows (Figure 1 g). Owing to the chemical affinity between DDT and hexyl side chains of P3HT-SH, minimal free DDT molecules may intercalate into the gap between adjacent hexyl chains from two neighboring P3HT chains, thereby strengthening the interaction of these hexyl side chains.[16] This in turn promotes P3HT-SH chains to grow (i.e., stack) along the direction of hexyl side chains (i.e., (100) direction; *a* axis in Figure 1 g), thus forming P3HT-SH nanoribbons.[14] A detailed exploration on the effect of DDT as additive on the P3HT crystallization is still ongoing and will be reported elsewhere. Notably, P3HT/Au nanoparticles (P3HT/AuNPs) hybrids in the nanofiber form have been obtained by electrospinning.[17] In contrast, nanoribbon-shaped P3HT/AuNRs nanocomposites produced in the present study were created via chemical bonding-directed hierarchical assembly in solution, which differ largely from electrospun P3HT/AuNPs nanofibers.[17]

The surface coverage of AuNRs within nanoribbon-shaped P3HT/AuNRs can be readily controlled by varying the concentration of AuNRs. As the concentration of AuNRs increased from 0.3 mM to 0.9 mM, AuNRs were observed to pack more densely and retain string-like end-to-end assembly with the decreased side-by-side and end-to-end distances between adjacent AuNRs (Figure 2). Such string-like end-to-end assembly of AuNRs may be ascribed largely to the fact that the density of -SH groups in the longitudinal direction of P3HT-SH nanoribbions (i.e., (010) direction, *b* axis in Figure 1 g) is higher than that of -SH groups on the transverse direction (i.e., (100) direction, *a* axis in Figure 1 g) due to the shorter average distance between two -SH groups in the longitudinal direction. Therefore, string-like end-to-end assembly of AuNRs along the longitudinal direction of P3HT-SH nanoribbons permits the formation of more Au-S bonding, thus minimizing the free energy of the system. In addition, it has been reported that the potential of anisotropic nanorods decays more rapidly near the tips so the directing of other nanorod is more energetically favorable towards the tip than the side of nanorod, which also favors the string-like conformation.[18]

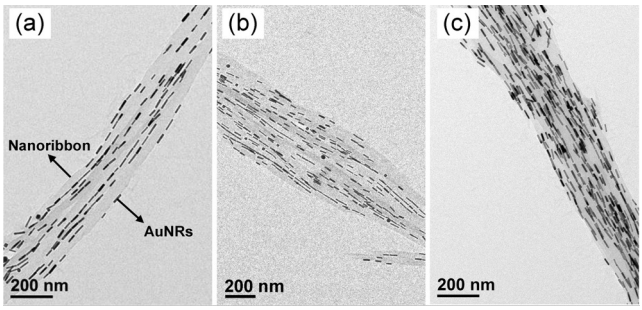

Figure 2. TEM images of nanoribbon-shaped P3HT/AuNRs nanocomposites composed of P3HT-SH nanoribbons and aligned plasmonic DDT-coated AuNRs (AuNRs-DDT) as a function of increased loading density (i.e., surface coverage) of AuNRs-DDT. The concentrations of AuNRs-DDT are a) 0.3 mM, b) 0.7 mM, and c) 0.9 mM.

It is interesting to note that AuNRs tend to adhere to P3HT-SH nanoribbons instead of P3HT-SH nanofibers. With the addition of AuNRs (length: 35.2 ± 2.8 nm, width: 12.6 ± 2.6 nm), most of P3HT-SH nanofibers transformed into nanoribbons due to the presence of minimal free DDT as a result of the dissociation of DDT from the surface of DDT-coated AuNRs as described above, with only few nanofibers remained (marked with arrows in Figure 3 a,b). When the loading of AuNRs on P3HT-SH nanoribbons was sufficiently high, free AuNRs (marked with circles in Figure 3 a) can be seen, while almost no AuNRs adhered to P3HT-SH nanofibers. For comparison, spherical Au nanoparticles (AuNPs) coated with DDT (12.8 ± 0.8 nm in diameter) were also synthesized (see Experimental Section in Supporting Information). Conversely, under the same situation of the coexistence of P3HT-SH nanofibers and nanoribbons, AuNPs were found to preferentially anchor at the edges of nanofibers rather than on the surface of nanoribbons (Figure 3 c,d). This clearly suggests that -SH groups are exposed at the edges of P3HT-SH nanofibers. We attribute such selective decorations (i.e., AuNPs populated at the edge of nanofiber and AuNRs situated on the surface of nanoribbon) to the different curvatures of AuNRs and AuNPs as well as their different contact areas available for interacting with P3HT-SH. The more Au–S interaction leads to the more stable assembled nanocomposites. Compared with AuNPs, AuNRs have larger volume and smaller curvature in the longitudinal direction.[13] When P3HT-SH nanofibers and nanoribbons are functionalized with the equal density of -SH groups, AuNPs possess larger spherical curvature and thus render more contacts with the curved and deformable nanofibers than with the flat nanoribbons. In contrast, the long axis of AuNRs with smaller curvature matches the planar geometry of nanoribbons well to maximize the Au–S chemical bonding.

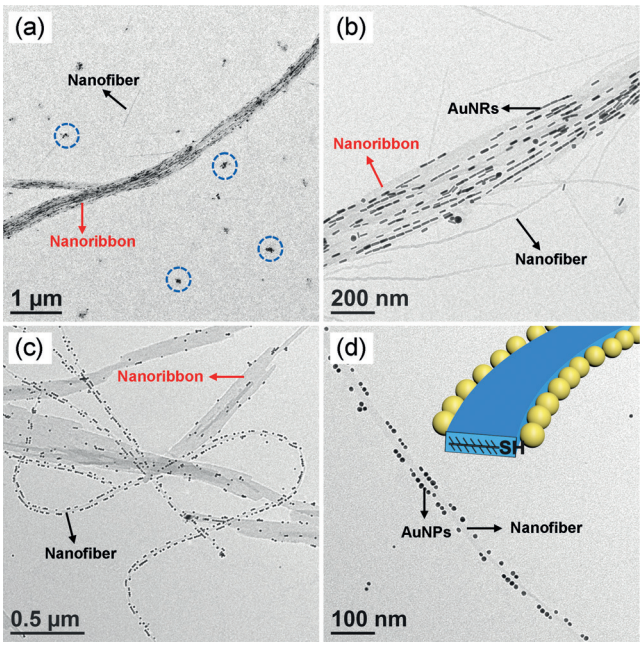

Figure 3. TEM images showing coexisting P3HT-SH nanoribbons and P3HT-SH nanofibers: a) and b) AuNRs-DDT selectively decorate P3HT-SH nanoribbons (marked with red arrows) rather than P3HT-SH nanofibers (marked with black arrows). Some free AuNRs are labeled with blue dashed circles in (a); they appear like nanoparticles due to the low resolution. c) and d) AuNPs-DDT selectively decorate P3HT-SH nanofibers instead of P3HT-SH nanoribbons. The inset in (d) is the corresponding schematic illustration of Au nanoparticles adhered to the edges of P3HT-SH nanofibers.

We note that the key to the success in forming hierarchical assembly of P3HT/AuNRs nanoribbons is the use of SH-terminated P3HT and the location of -SH groups at the edge of P3HT-SH nanofibers. For comparison, P3HT nanofibers without -SH end groups were also employed and mixed with AuNRs-DDT. It is not surprising that due to the presence of the minimal free DDT as discussed above, some P3HT nanofibers were still transformed into nanoribbons but without the anchoring of AuNRs on the surface owing to the absence of Au–S interaction (Figure S6). Moreover, when the molecular weight of P3HT-SH was higher than 10 kDa, significant phase segregation of P3HT-SH nanofibers and AuNRs was observed and no hierarchical assembly of P3HT/AuNRs nanoribbons was formed (Figure S7). In this case (i.e., $M_n = 12$ kDa $> M_{n,C} = 10$ kDa), P3HT-SH backbones underwent chain folding and led to the -SH end groups embedded within the nanofibers instead of being exposed at their edges. This hinders the contact between AuNRs and -SH groups to form Au–S bonding. In addition to the studies noted above, control experiment also showed that when P3HT-SH nanofibers were first transformed into nanoribbons upon the addition of excess DDT, followed by mixing with AuNRs-DDT, no nanoribbon-like nanocomposites were observed (Figure S8). This may be due to the aggregation of nanoribbons with each other, which impeded the Au–S interaction.

To explore optical properties of P3HT/AuNRs nanoribbons and their respective constituents, UV/Vis and photoluminescence (PL) measurements were performed (Figure 4).

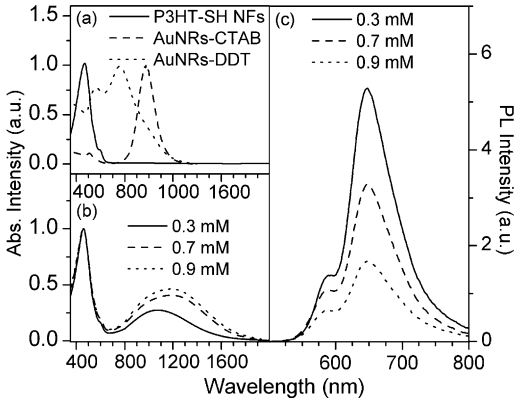

Figure 4. a) UV/Vis absorption spectra of P3HT-SH nanofibers (NFs), AuNRs-CTAB, and AuNRs-DDT solutions. b) UV/Vis absorption and c) Photoluminescence (PL) spectra of nanoribbon-shaped P3HT/AuNRs nanocomposites formed by a co-assembly of P3HT-SH nanofibers into P3HT-SH nanoribbons and AuNRs-DDT aligned on the surface of nanoribbon at different AuNRs-DDT concentrations.

For the P3HT-SH nanofiber $CH_2Cl_2/CHCl_3$ solution, a main absorption peak at 468 nm and a vibronic peak at 597 nm were seen, which are due to the intrachain π–π* transition of P3HT backbone and the interchain π–π interaction, respectively (Figure 4a). The AuNRs-CTAB water solution exhibited transverse (TSPR) and longitudinal (LSPR) surface plasmon resonance at 506 nm and 976 nm, respectively (Figure 4a). It has been shown that in AuNR system, the side-by-side interactions between adjacent AuNRs lead to a red-shift of TSPR and a blue-shift of LSPR, while the end-to-end arrangement red-shifts both bands.[19] After the ligand-exchange of AuNRs-CTAB with DDT, the TSPR of the resulting AuNRs-DDT red-shifted to 558 nm and the LSPR blue-shifted to 760 nm, signifying the side-by-side assembly of AuNRs-DDT (Figure 4a) which is in good agreement with the TEM observation (Figure 1c). When AuNRs-DDT interact with P3HT-SH to form nanoribbon-shaped P3HT/AuNRs nanocomposites, the appearance of characteristic P3HT and AuNR absorption peaks indicated the successful and effective binding between these two components. The LSPR of AuNRs-DDT ($c = 0.3$ mM) red-shifted to 1080 nm because of the end-to-end assembly of AuNRs that were aligned along nanoribbons (Figure 4b), which is clearly evident in TEM image (Figure 2a). With the increased loading of AuNRs-DDT (i.e., higher AuNRs-DDT concentration), the LSPR became notably broadened due to plasmon coupling at reduced interparticle distance, and it further red-shifted to 1190 nm (Figure 4b; $c = 0.9$ mM).

Figure 4c shows the PL spectra of the P3HT/AuNRs nanoribbon $CH_2Cl_2/CHCl_3$ solution at different AuNRs-DDT concentrations. The P3HT-SH within these nanoribbon-shaped nanocomposites exhibited two emission peaks at 589 nm and 647 nm, corresponding to the 0–0 and 0–1 singlet transitions, respectively. It is well known that the PL quenching is often observed when fluorophores are in close proximity to a metal surface.[20] It is clear that with the increased loading density of AuNRs from 0.3 mM to 0.9 mM, the PL of P3HT-SH was gradually decreased. The PL

quenching may be rationalized in the following. With the increased surface coverage of P3HT-SH nanoribbons by AuNRs, the holes in P3HT-SH are likely to be effectively transferred to AuNRs due to their close energy levels (valence band of P3HT is 5.2 eV,[21] and the Fermi level of Au is 5.1 eV[22]), thereby reducing the recombination of photoexcited electrons and holes in P3HT-SH, and thus decreasing the PL of P3HT.

In summary, we developed a facile bottom-up co-assembly strategy for crafting hierarchical nanoribbon-shaped P3HT/AuNR nanocomposites composed of a P3HT-SH nanoribbon and aligned AuNRs-DDT on the surface of the nanoribbon. Such assembly was triggered by the presence of minimal free DDT which had dissociated from the AuNRs surface and drives the transformation of P3HT-SH nanofibers into nanoribbons, accompanied by the AuNRs aligning along the long axis of nanoribbons via the formation of Au–S bonds. These P3HT/AuNRs nanocomposites exhibited the typical broadened and red-shifted absorptions of AuNRs in the near infrared region due to the plasmon coupling of adjacent AuNRs, and gradually decreased PL of P3HT with the increased surface coverage of P3HT by AuNRs. We envision that this simple yet effective strategy may be extended to produce hierarchically assembled nanocomposites comprising other conjugated polymers and functional nanorods with unique catalytic, sensing, optical, electronic, and optoelectronic properties.

Acknowledgements

This work was financially supported by the National Natural Science Foundation of China (Grant No. 21274029).

Keywords: gold nanorods · co-assembly · nanocomposites · nanoribbons · poly(3-hexylthiophene)

How to cite: *Angew. Chem. Int. Ed.* **2016**, *55*, 8686–8690
Angew. Chem. **2016**, *128*, 8828–8832

[1] J. Kao, K. Thorkelsson, P. Bai, B. J. Rancatore, T. Xu, *Chem. Soc. Rev.* **2013**, *42*, 2654–2678.
[2] J. L. Wu, L. T. Weng, W. Qin, G. D. Liang, B. Z. Tang, *ACS Macro Lett.* **2015**, *4*, 593–597.
[3] L. Zhao, Z. Q. Lin, *Adv. Mater.* **2012**, *24*, 4353–4368.
[4] a) M. Shin, J. Y. Oh, K. E. Byun, Y. J. Lee, B. Kim, H. K. Baik, J. J. Park, U. Jeong, *Adv. Mater.* **2015**, *27*, 1255–1261; b) S. Samitsu, T. Shimomura, S. Heike, T. Hashizume, K. Ito, *Macromolecules* **2008**, *41*, 8000–8010; c) Z. Yu, H. Yan, K. Lu, Y. J. Zhang, Z. X. Wei, *RSC Adv.* **2012**, *2*, 338–343.
[5] a) L. Zhao, X. C. Pang, R. Adhikary, J. W. Petrich, M. Jeffries-EL, Z. Q. Lin, *Adv. Mater.* **2011**, *23*, 2844–2849; b) L. Zhao, X. C. Pang, R. Adhikary, J. W. Petrich, Z. Q. Lin, *Angew. Chem. Int. Ed.* **2011**, *50*, 3958–3962; *Angew. Chem.* **2011**, *123*, 4044–4048.
[6] F. A. Bokel, P. K. Sudeep, E. Pentzer, T. Emrick, R. C. Hayward, *Macromolecules* **2011**, *44*, 1768–1770.
[7] L. Vigderman, B. P. Khanal, E. R. Zubarev, *Adv. Mater.* **2012**, *24*, 4811–4841.
[8] a) Z. P. Wang, A. G. Skirtach, Y. Xie, M. Y. Liu, H. Möhwald, C. Y. Gao, *Chem. Mater.* **2011**, *23*, 4741–4747; b) E. B. Pentzer, F. A. Bokel, R. C. Hayward, T. Emrick, *Adv. Mater.* **2012**, *24*, 2254–2258.
[9] K. Okamoto, C. K. Luscombe, *Chem. Commun.* **2014**, *50*, 5310–5312.
[10] J. H. Liu, M. Arif, J. H. Zou, S. I. Khondaker, L. Zhai, *Macromolecules* **2009**, *42*, 9390–9393.
[11] X. C. Ye, C. Zheng, J. Chen, Y. Z. Gao, C. B. Murray, *Nano Lett.* **2013**, *13*, 765–771.
[12] A. Wijaya, K. Hamad-Schifferli, *Langmuir* **2008**, *24*, 9966–9969.
[13] W. K. Li, P. Zhang, M. Dai, J. He, T. Babu, Y. L. Xu, R. H. Deng, R. J. Liang, M. H. Lu, Z. H. Nie, J. T. Zhu, *Macromolecules* **2013**, *46*, 2241–2248.
[14] G. H. Lu, L. G. Li, X. N. Yang, *Adv. Mater.* **2007**, *19*, 3594–3598.
[15] D. S. Sidhaye, B. L. V. Prasad, *Chem. Mater.* **2010**, *22*, 1680–1685.
[16] H. Y. Wang, J. G. Liu, Y. C. Han, *Polymer* **2013**, *54*, 948–957.
[17] H. C. Chang, C. L. Liu, W. C. Chen, *Adv. Funct. Mater.* **2013**, *23*, 4960–4968.
[18] M. A. Correa-Duarte, J. Pérez-Juste, A. Sánchez-Iglesias, M. Giersig, L. M. Liz-Marzán, *Angew. Chem. Int. Ed.* **2005**, *44*, 4375–4378; *Angew. Chem.* **2005**, *117*, 4449–4452.
[19] C. L. Zhang, K. P. Lv, H. P. Cong, S. H. Yu, *Small* **2012**, *8*, 648–653.
[20] S. T. Kochuveedu, D. H. Kim, *Nanoscale* **2014**, *6*, 4966–4984.
[21] S. Das, T. L. Alford, *J. Appl. Phys.* **2014**, *116*, 044905.
[22] T. Bora, H. H. Kyaw, S. Sarkar, S. K. Pal, J. Dutta, *Beilstein J. Nanotechnol.* **2011**, *2*, 681–690.

Received: March 31, 2016
Published online: May 17, 2016

